lubricants

MDPI

Article

Effects of Oil and Solid Body Temperatures on Elastohydrodynamic Lubrication Film Formation

Junbin Gao [1], Ping Yang [1], Xinming Li [1,2,*], Xuyang Jin [1], Ye Tian [1], Ziyang Cheng [1] and Xu Yan [1]

[1] School of Mechanical & Automotive Engineering, Qingdao University of Technology, 777 Jialingjiang Road, Qingdao 266520, China; gaojunbin1998@163.com (J.G.); yp_qingdao@163.com (P.Y.); xuyangjin2021@163.com (X.J.); yetian990902@163.com (Y.T.); chengziyang9340@163.com (Z.C.); yxynl1999@163.com (X.Y.)

[2] Shandong Zhilian Community Bearing Technology Co., Ltd., Liaocheng 252600, China

* Correspondence: lixinming@qut.edu.cn; Tel.: +86-18660261702

Abstract: The present study focuses on investigating the influence of oil and solid body temperatures on elastohydrodynamic lubrication (EHL) film formation. Experimental and numerical simulation methods are employed to examine three heating methods: oil and ball heating, disc heating, and entire system heating. A preliminary comparison between the measured results and numerical simulations confirms the impact of heating methods on film formation while validating the availability of the numerical models. Further numerical analysis reveals that in the case of oil and ball heating, the temperature gradient induced by differences in solid body temperatures plays a more significant role in film formation compared to the conventional thermal-viscosity wedge effect caused by EHL film shear. This effect is further amplified at large sliding–rolling ratios and in steel–steel contacts. The overall film formation is primarily governed by the oil inlet temperature, whereas local film formation characterized by a dimple shape is influenced by both thermal gradient effects and thermal-viscosity wedge effects. This study provides valuable insights for selecting appropriate heating methods in experiments as well as understanding how temperature differences affect film formation in practical engineering.

Keywords: elastohydrodynamic lubrication; temperature gradient; thermal-viscosity wedge; film formation

Citation: Gao, J.; Yang, P.; Li, X.; Jin, X.; Tian, Y.; Cheng, Z.; Yan, X. Effects of Oil and Solid Body Temperatures on Elastohydrodynamic Lubrication Film Formation. *Lubricants* **2024**, *12*, 28. https://doi.org/10.3390/lubricants12020028

Received: 25 December 2023
Revised: 18 January 2024
Accepted: 19 January 2024
Published: 23 January 2024

1. Introduction

The concentrated contacts encountered in mechanical components such as rolling bearings, cam-followers, and gears commonly operate under rolling–sliding conditions and within the regime of elastohydrodynamic lubrication (EHL). In EHL contacts, the lubricating films experience both high normal pressure and high tangential shear rate. The high normal pressure leads to an exponential increase in lubricant viscosity and surface deformation, thereby providing both travel time and accommodation space for the lubricant. The combination of high viscosity and high shear rate results in an increase in viscous friction, which serves as one of the primary sources of heat generation within the lubrication system. Other sources contributing to heat generation, e.g., in high-speed rolling bearings, include the inlet reverse flow, lubricant churning in bearing cavities, as well as friction between rolling element cages. The generated heat propagates through the bearings, inducing alterations in the temperature field, thereby exerting an influence on the overall performance of rolling bearings [1], the limiting speed [2], and even their service life [3]. Therefore, the measurement of temperature rise has been widely adopted as an important parameter in bearing tests for evaluating lubrication properties [4,5] and serves as a failure criterion for lubricants or rolling bearings [6,7].

The temperature feedback resulting from heat generation and dissipation in the overall system leads to a decrease in lubrication viscosity, thereby weakening the film formation ability and influencing the rheological properties of the EHL films. To investigate the

impact of temperature on film formation and the rheological behaviors of EHL films under thermal effects, numerous model tests and numerical simulations were conducted using ball-on-disc or twin disc configurations [8–11]. In the majority of studies, it is commonly assumed that the entire system reaches a state of equilibrium, i.e., the ambient temperatures of the glass disk, steel ball, and lubricant are equal. In experimental tests, the steel ball was typically immersed in heated oil [10,12] or the heated oil was injected into the contact pairs, facilitating the measurement of the film thickness or friction coefficient at different temperatures [13,14]. Essentially, given the contact geometry, speed, load, and with an adequate lubricant supply, the film formation is primarily determined by the inlet lubricant viscosity, which is a function of the ambient temperature [15]. Once entering the highly pressured contacts, the lubricant exhibits non-Newtonian behaviors such as shear thinning [16] and thermal thinning [17]. By employing optical interferometry, the thermal-effect-induced abnormal film feature known as the dimple was visualized under conditions of a large sliding–rolling ratio (SRR) [18–20]. The thermal thinning effect leads to a decrease in the friction coefficient, particularly at high loads, as the SRR increases [11,12,14,21].

In numerical simulations, extensive investigations have been conducted on the film thickness, pressure, and temperature distributions, as well as the friction coefficient in thermoelastohydrodynamic lubrication (TEHL) contacts [9,22–25]. The occurrence of dimples in TEHL contacts was also observed [20,26,27], and the factors governing the size and locations of these dimples were identified [18–20,28]. Remarkable dimples can be formed under high-SRR conditions, such as during simple disc sliding or even when there is an opposite motion between contact surfaces [20,27,29]. Although these kinematic conditions may not be common in practical scenarios, they do provide evidence for the existence of thermal effects and their corresponding influence on EHL formation. Recently, an infrared microscopy technique has been developed to accurately map temperature distributions on both bounding surfaces and throughout the thickness of EHL films [29–31].

The dimple phenomena were interpreted using an acceptable thermal-viscosity wedge effect [26], based on both numerical simulations [20,27,29] and experimental observations [18,19,28]. According to this phenomenon, the thermal conductivity of bounding surfaces plays a crucial role in determining dimple formation [32]. Consequently, it induces a temperature difference between the two bounding surfaces, resulting in the establishment of a viscosity gradient across the lubrication film. This implies that both TEHL behaviors [33–35] and film traction [14,32] are influenced by the solid body temperature. In fact, during model tests or practical engineering applications, the utilization of the asymmetry heating method or asymmetry heating transfer process can result in significant temperature differences between bounding surfaces. In principle, if these temperature differences align with the establishment of a thermal-viscosity wedge effect, it will enhance this effect; conversely, it will weaken the effect in the opposite case. The aim of this research is thus to validate whether these assumptions are true through model tests and numerical simulations.

The term ‘asymmetry heating method’ used in this study refers to a heating method that differs from the conventional system-wide heating method, where the temperatures of both the lubricant at the inlet zone and bounding surfaces are at equal. The heating methods are described in the next section. The impact of heating methods on the EHL film formation is experimentally observed. Extensive numerical simulations are conducted to compare the influence of the temperature difference induced by heating methods on the thermal-viscosity wedge effect and consequently the film formation. This study helps in the comprehension of the combined impact of bounding surface temperature and the thermal-viscosity wedge effect on film formation, as well as aids in selecting an appropriate heating method in tests.

2. Test Apparatus and Heating Methods

Experimental investigations were conducted using an optical EHL film test apparatus featuring a ball-on-disc configuration, as illustrated in Figure 1. The steel ball is loaded

against a glass disc with a chromium-coated layer on the contact side. The glass disc and steel ball are independently driven by the servo motor, enabling the attainment of different entrainment velocities and SRRs. A dual-beam laser light source that compresses red and green colors is incident on the contact point, forming a colorful interferogram. The magnified image through the microscope is captured by a Charge-Coupled Device (CCD) and stored on a computer for subsequent analysis. The film thickness and profile can be reconstructed utilizing dedicated software DIIM-2015 [36].

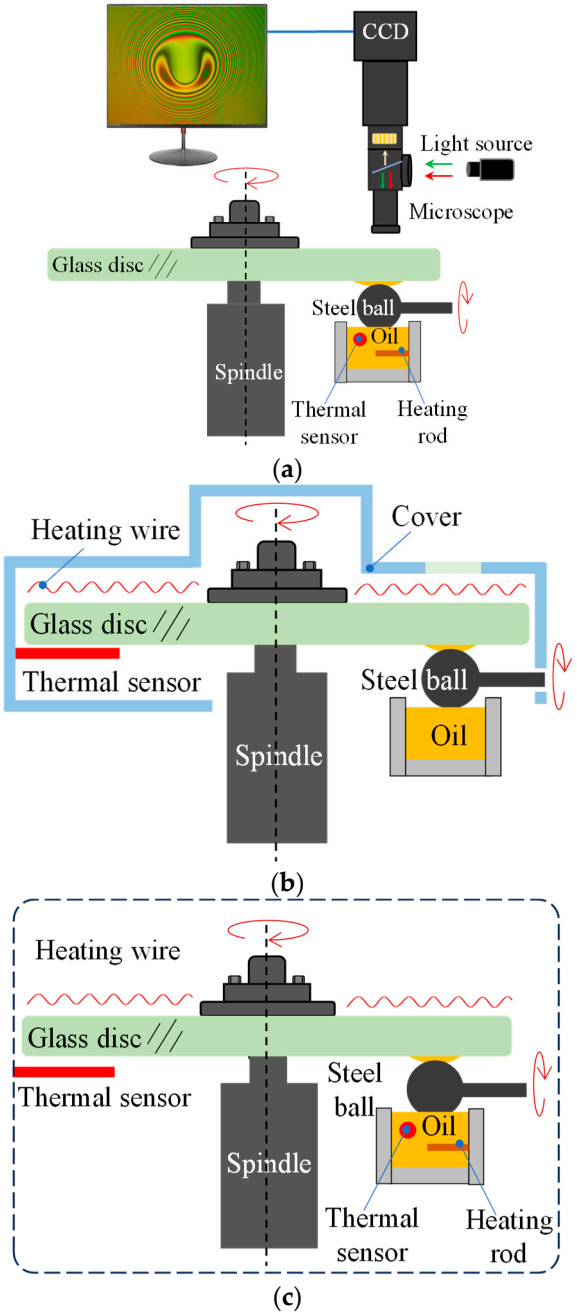

Figure 1. Schematic diagram of test apparatus and heating methods. (**a**) Oil and ball heating, (**b**) glass disc heating, (**c**) system heating.

The heating approach depicted in Figure 1a involves immersing a steel ball partially in a small oil container, with a heating rod inserted. As a result of thermal conduction, both the oil and the immersed portion of the steel ball are heated. It is important to note that this experimental setup lacks isolation from its surroundings, resulting in the

glass disc being exposed to room temperature controlled by air conditions. Consequently, this method results in higher temperatures on the surface of the ball compared to that of the glass surface. The temperature is measured and regulated using a thermal sensor, ensuring the maintenance of the desired oil temperature. The thermal sensor is positioned perpendicularly to the heating rod, which is visually indicated as a red dot in Figure 1a. The tailored heating wire is positioned on the top glass surface in Figure 1b, with a small window reserved for the microscope lens. A cover is utilized to minimize heat dissipation to the surroundings. This approach eliminates the need for heating components in oil, resulting in a higher temperature of the glass surface than that of the ball surface. To ensure uniform heating, the glass disc should rotate at a low speed during the heating process. By combining the heating approaches depicted in Figure 1a,b, along with the utilization of a large insulating cover, the entire system can be uniformly heated. In this heating method, two thermal sensors are employed to measure temperatures of both the disc and oil separately. It is anticipated that the glass disc, steel ball, and oil will attain an equal temperature. The heating methods illustrated in Figure 1a,b are referred to as asymmetrical heating methods, while the method shown in Figure 1c represents a symmetrical heating method. Prior to each experiment, preheating is conducted until the desired temperature is achieved.

The temperature range in the tests spans from t_0 = 25 °C to 75 °C. The lubricant used is FVA3, and its properties are listed in Table 1. Viscosity measurements of FVA3 are conducted at different temperatures using a rheometer (Anton Paar, MCR 302), and the resulting data are presented in Figure 2. The viscosities at t_0 = 25 °C, 50 °C, and 75 °C are η_0 = 0.2 Pa·s, 0.05 Pa·s, and 0.0175 Pa·s, respectively. The SRR is defined as SRR = $(u_d - u_b)/u_e$, where $u_e = (u_d + u_b)/2$ represents the entrainment speed.

Table 1. Properties of FVA 3.

Parameters	Specification
Density at 22 °C, ρ_0, kg/m^3	875
Viscosity at 22 °C, η_0, Pa·s	0.23
Specific heat of lubricant, c, J/kg·K	2000
Thermal conductivity of lubricant, k, W/m·K	0.14

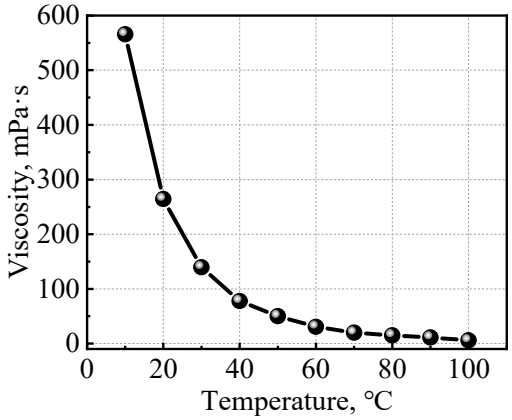

Figure 2. Variations in viscosity with temperature.

3. Numerical Model and Governing Equations

The numerical model used in the simulations is depicted in Figure 3. The velocities of the steel ball and glass disc are represented as u_b and u_d, respectively. The calculated domain is from x_{in} to x_{out}. At $x = x_{in}$, the temperatures of steel and glass are t_b and t_d, respectively, while the inlet oil temperature is denoted as t_0. The parameters for the lubricant and the contact pair can be found in Table 2.

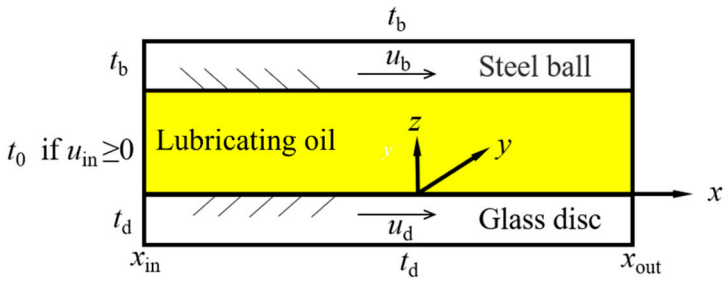

Figure 3. Schematic diagram of temperature boundary of glass disc, steel ball, and lubricant.

Table 2. Parameters of the lubricant and contact pair.

Parameters	Specification
Specific heat of oil, c, J/kg·K	2000
Density of oil, ρ, kg/m^3	875
Thermal conductivity of oil, k, W/m·K	0.14
Effective modulus of steel–glass contact, E', GPa	123.9
Specific heat of glass, c_d, J/kg·K	840
Specific heat of steel, c_b, J/kg·K	470
Density of glass, ρ_d, kg/m^3	2500
Density of steel, ρ_b, kg/m^3	7850
Thermal conductivity of glass, k_d, W/m·K	0.84
Thermal conductivity of steel, k_b, W/m·K	46

3.1. Temperature-Governing Equations

Using the coordinates established in Figure 3 and neglecting the thermal conduction terms in x and y directions, the energy equation of EHL films can be written as

$$c\left[\rho u\frac{\partial t}{\partial x}+\rho v\frac{\partial t}{\partial y}-\left(\frac{\partial}{\partial x}\int_0^z \rho u dz'+\frac{\partial}{\partial y}\int_0^z \rho v dz'\right)\frac{\partial t}{\partial z}\right]=k\frac{\partial^2 t}{\partial z^2}-\frac{t}{\rho}\frac{\partial \rho}{\partial t}\left(u\frac{\partial \rho}{\partial x}+v\frac{\partial \rho}{\partial y}\right)+\phi \quad (1)$$

where Φ is the heat dissipation item, which can be expressed as $\phi=\eta^*\left[\left(\frac{\partial u}{\partial z}\right)^2+\left(\frac{\partial v}{\partial z}\right)^2\right]$.

The energy equations for the glass disc and steel ball can be written as

$$\begin{cases} c_b\rho_b u_b\frac{\partial t}{\partial x}=k_b\frac{\partial^2 t}{\partial z_b^2} \\ c_d\rho_d u_d\frac{\partial t}{\partial x}=k_d\frac{\partial^2 t}{\partial z_d^2} \end{cases} \quad (2)$$

where z_b and z_d lie along the z-axis direction.

On the two oil–solid interfaces, the heat flux continuity must be satisfied as

$$\begin{cases} k_b\frac{\partial^2 t}{\partial z_d^2}\Big|_{z_d=0}=k\frac{\partial t}{\partial z}\Big|_{z=0} \\ k_b\frac{\partial^2 t}{\partial z_b^2}\Big|_{z_b=0}=k\frac{\partial t}{\partial z}\Big|_{z=h} \end{cases} \quad (3)$$

The lubricant boundary condition is

$$t(x_{in},y,z)=t_0(u_{in}\geq 0) \quad (4)$$

where u_{in} represents the inlet velocity of oil. In the case of $u_{in} < 0$, indicating a reverse flow region and other boundaries, no boundary condition is required.

The boundary conditions of the glass disc and steel ball are written as

$$\begin{cases} t(x_{in},y,z_d)=t_d, t(x_{in},y,-d)=t_d \\ t(x_{in},y,z_b)=t_b, t(x_{in},y,d)=t_b \end{cases} \quad (5)$$

where d is the temperature domain of the glass disc and steel ball, in which the temperature changes across its thickness. The thickness of d is $d = 3a$, where a is the Hertz contact radius.

3.2. Non-Newtonian Rheological Model

The Eyring rheological model is used and can be expressed as [37]

$$\eta = \eta_0 \frac{ln\left(\frac{\eta_0\dot{\gamma}}{\tau_0} + \sqrt{\left(\frac{\eta_0\dot{\gamma}}{\tau_0}\right)^2 + 1}\right)}{\frac{\eta_0\dot{\gamma}}{\tau_0}} \quad (6)$$

where η_0 is the ambient viscosity of the lubricant, τ_0 is the Eyring shear stress, and τ_0 = 10 MPa.

The remaining equations, including the generalized Reynolds equation, film thickness equation, density relation, viscosity relation, and loading balance, are consistent with those found in the literature [37] and are not listed here.

3.3. Numerical Solutions

The numerical solution is obtained through an iterative process involving the pressure and temperature fields. The multi-grid method is employed to solve the pressure, while the surface elastic deformation caused by pressure is addressed using the multi-grid integration method. Additionally, the energy equation is solved using a column scanning approach. Given that the contact region exhibits symmetry about the *X*-axis, a semi-domain solution is adopted for numerical calculations.

4. Results and Discussion

4.1. Comparisons of Test Results and Simulations

The experimental interferograms and numerical pseudo-interferograms under three heating methods are presented in Figure 4. For each heating method, the left color images represent the experimental results, while the black and white images on the right side depict the numerical simulation results. In all three cases, a nominal temperature of 75 °C is applied when heating the oil, glass disc, or steel ball; otherwise, a nominal temperature of 25 °C is maintained.

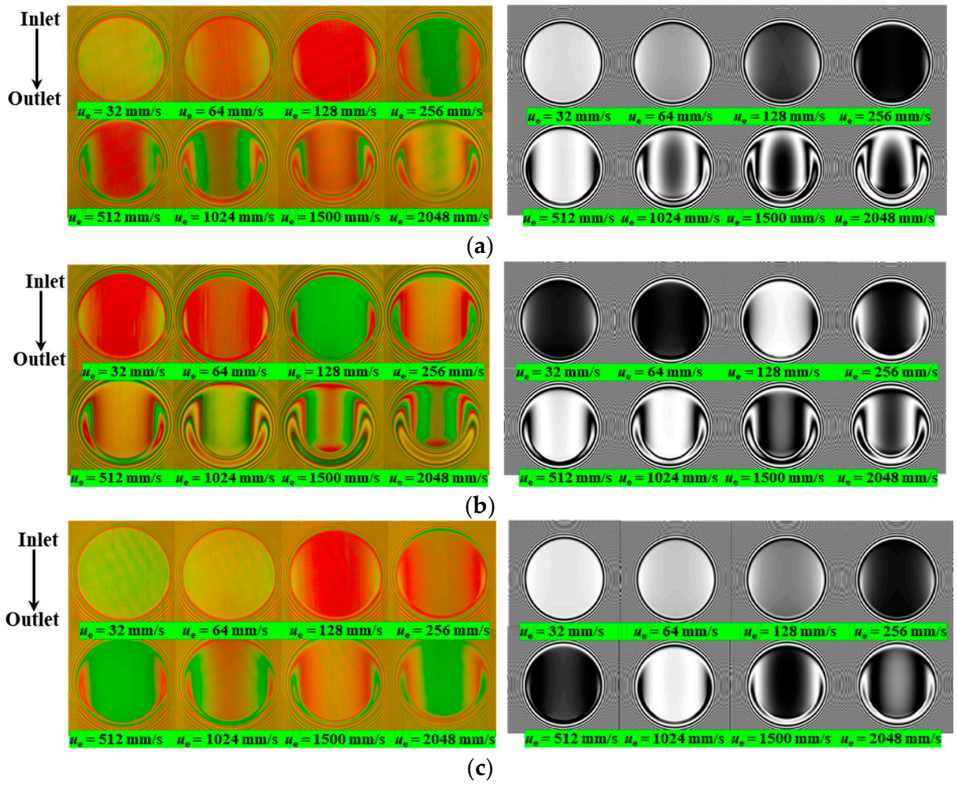

Figure 4. Comparisons of experimental interferograms and numerical pseudo-interferograms under different heating methods, p_H = 0.7 GPa, SRR = 0.5. (**a**) Oil and steel ball heating, $t_0 = t_b$ = 75 °C, t_d = 25 °C; (**b**) glass disc heating, $t_0 = t_b$ = 25 °C, t_d = 75 °C; (**c**) entire system heating, $t_0 = t_b = t_d$ = 75 °C.

From the images in Figure 4, it is evident that as the entrainment velocity increases, the contacts exhibit typical horseshoe EHL features. In the case of the oil and steel ball heating method (Figure 4a), a slight dimple is observed near the outlet constriction at a speed of u_e = 2048 mm/s in the experimental image. On the right side of the numerical image, the dimple appears at u_e = 1024 mm/s and becomes more pronounced with increasing speed. Moreover, when the speed exceeds 1024 mm/s, an incipient large dimple forms at the center of the contact. Both experimental and numerical images show noticeable dimples at elevated speeds for the disc heating method. Conversely, no dimples are observed for the entire system heating method and the numerical images closely match the experimental results. The appearance of dimples indicates that the thermal-viscosity wedge plays a role in local film formation.

The central film thickness of experimental measurements and numerical simulations is quantitatively compared in Figure 5. Overall, the measured film thicknesses (the blue symbols are error bar) are higher than those predicted numerically in all three cases. This discrepancy can be attributed to the instability of temperature control during the tests. Due to heat dissipation to the surroundings, the experimental temperatures are actually lower than nominal temperatures, causing a higher viscosity and consequently thicker film thickness. The film thicknesses measured in Figure 5a,b approach the numerical values at higher speeds. This observation may be attributed to the occurrence of starvation due to high centrifugal force, despite the oil–air boundary at the inlet not being within the field of view. Disc heating leads to more significant heat dissipation, resulting in considerably higher measured film thicknesses even at elevated speeds. Throughout the tests, disc temperature was continuously monitored and recorded. The actual temperatures corresponding to different speeds are presented in Table 3. It is evident that as the speed increases, there is a substantial decrease in actual temperature. This could potentially be due to incomplete closure of the ball and oil tank sides by a cover, allowing air churning at high speeds which accelerates airflow and enhances heat dissipation. By utilizing the viscosities listed in Table 3 as input parameters, the predicted film thicknesses (represented by the green curve in Figure 5b) approach those obtained through measurement.

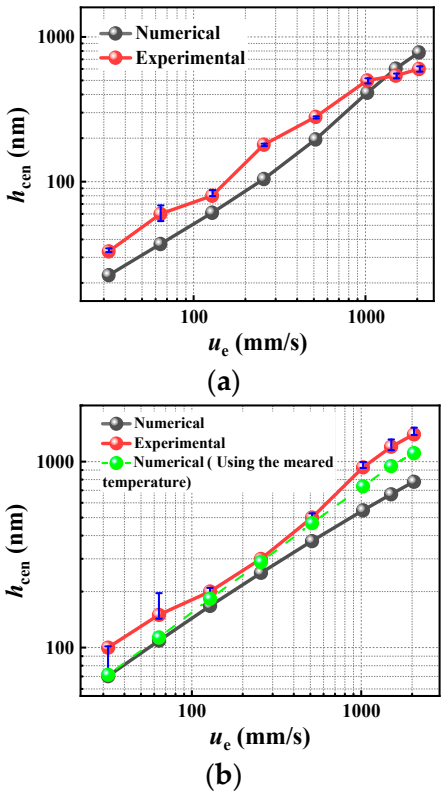

Figure 5. *Cont.*

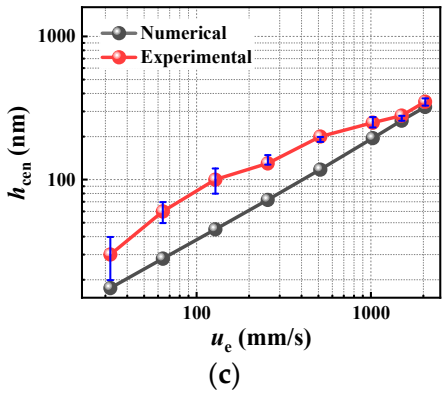

Figure 5. Comparisons of the central film thickness between experimental measurement and numerical simulation under three heating methods, p_H = 0.7 GPa, SRR = 0.5. (**a**) Oil and steel ball heating, $t_0 = t_b$ = 75 °C, t_d = 25 °C; (**b**) glass disc heating, $t_0 = t_b$ = 25 °C, t_d = 75 °C; (**c**) entire system heating, $t_0 = t_b = t_d$ = 75 °C.

Table 3. Measured temperature at different speeds.

Velocity (mm/s)	32	64	128	256	512	1024	1500	2048
Temperature of disc (°C)	68	64	56	52	46	43	40	40

According to the classical Hamrock–Dowson formula [38], the group of ($\eta_0 u_e$) plays a crucial role in film formation, where the inlet ambient viscosity η_0 is a key factor to determine the film thickness. It should be noted that in Figure 5a, despite the significantly lower η_0 at 75 °C compared to Figure 5b at 25 °C (see Figure 3), the film thickness in Figure 5a remains considerable and comparable between the two cases. The underlying mechanism is further discussed in the subsequent text. The results in Figure 5 substantiate the applicability of the numerical model for predictions and lend support to the subsequent analysis.

4.2. Numerical Simulation of Oil and Solid Body Temperatures on EHL Film Formation

To investigate the influence of oil and body temperatures on EHL films numerically, Figure 6 illustrates the variations in central film thickness with entrainment speed under different SRRs. The temperatures of both the oil and contact bodies are set according to the experimental heating methods employed. To facilitate comparisons between the curves under different conditions, the linear–linear scale is employed instead of the log–log scale. In Figure 6a, where the oil and ball temperatures exceed that of the disc surface, an artificial temperature gradient is induced across the oil film, consequently resulting in a viscosity gradient as well. The term 'temperature gradient' is specifically employed in subsequent analysis to differentiate it from the conventional thermal viscosity wedge mechanism that occurs spontaneously due to oil shear, thereby describing the mechanism resulting from temperature differences between the contacting bodies. It should be noted that this situation differs from the thermal viscosity wedge mechanism, wherein the disc surface temperature is higher than that of the ball surface. The external imposed temperature gradient acts as a counteractive mechanism against the thermal effect generated by the film itself, even becoming the dominant factor governing film formation. The higher the SRR, particularly at elevated speeds, the higher the overall film thickness. This is attributed to thick oil being entrained into the contacts by the disc surface due to its lower temperature while thin oil is entrained by the hot ball surface. According to the definition of the SRR, a larger value indicates a faster disc surface speed and greater entrainment of thick oil into the contacts, thus contributing significantly to film formation. Furthermore, the oil temperature in this case is obviously higher than that depicted in Figure 6b, resulting in a much lower inlet viscosity. This unfavorable condition inhibits the establishment of an EHL film, which emphasizes the profound influence of the external temperature gradient on film formation.

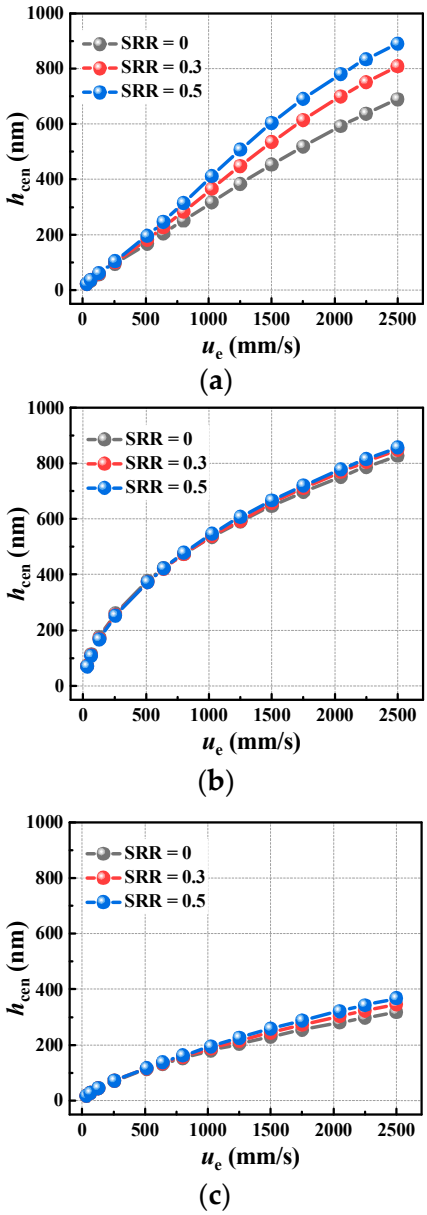

Figure 6. Effect of oil and temperatures on film thickness under different SRRs, p_H = 0.7 GPa. (**a**) Oil and steel ball heating, $t_0 = t_b$ = 75 °C, t_d = 25 °C; (**b**) glass disc heating, $t_0 = t_b$ = 25 °C, t_d = 75 °C; (**c**) entire system heating, $t_0 = t_b = t_d$ = 75 °C.

In Figure 6b, it is evident that a lower oil temperature enables a higher inlet oil viscosity, which dominates the overall establishment of film thickness. Despite the imposition of an external temperature gradient and alignment with the conventional thermal-viscosity wedge mechanism, where the temperature of the glass disc surface is higher, no obvious differences are recognized among the curves at the three SRRs. This can be mainly attributed to the lower ball speed than that of the glass surface at SRR = 0.3 and SRR = 0.5, with even lower speeds associated with higher SRR values. The reduced ball speed weakens the entrainment effect of thick oil into contacts, thereby reducing the significance of the thermal-viscosity wedge effect.

In the case of Figure 6c, a significant reduction in film thickness is observed due to the low viscosity of the inlet oil and the absence of an external temperature gradient. Only a regular thermal-viscosity wedge effect induced by in-contact shear is generated. This results in a higher oil viscosity near the steel surface but lower viscosity near the glass surface. This thermal-viscosity wedge effect is further enhanced by a higher SRR, thereby contributing to film formation to some extent.

To comprehensively investigate the influence of the inlet oil temperature and temperature difference on film formation, Figure 7 further compares the film thickness under three heating

methods. It is evident that regardless of oil and ball heating, disc heating, or entire system heating, the overall film thickness significantly decreases compared to the case where $t_0 = t_b = t_d = 25$ °C. In Figure 7a, under a fixed disc temperature of 25 °C, the temperatures of the oil and steel ball increase. The observed variations in curves depend on the inlet ambient viscosity determined by the oil temperature. However, in Figure 7c under similar inlet ambient viscosities, there is a sharp reduction in film thickness to lower magnitudes. This confirms the effect of the temperature gradient on countering the decrease in film thickness induced by oil heating. Furthermore, increasing temperature differences will enhance this gradient effect and slow down the reduction in film thickness. In Figure 7b, both inlet ambient viscosity and heat transfer from the disc primarily determine the film thickness, since the impact of the temperature gradient effect is less significant, as shown in Figure 6b.

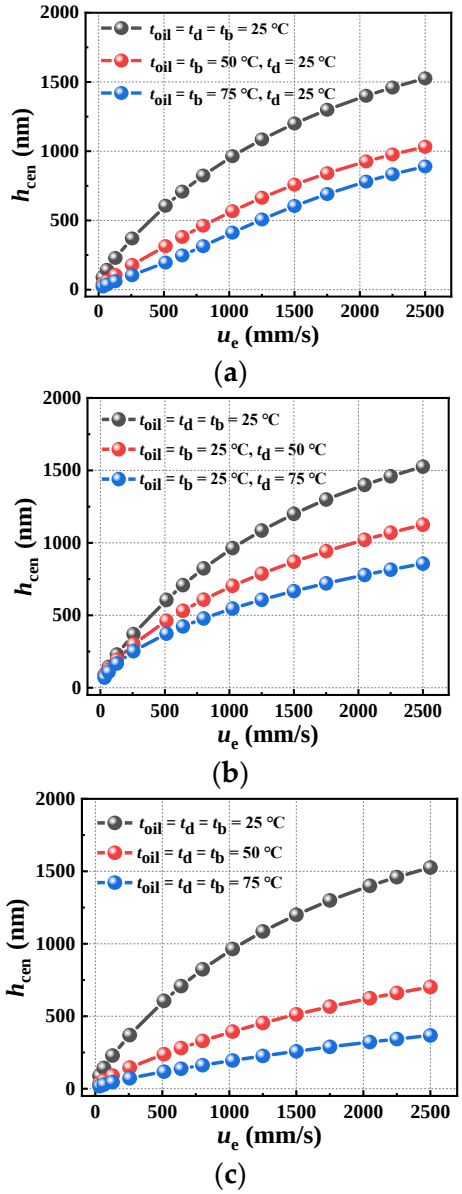

Figure 7. Heating methods on film thickness under different SRR = 0.5, $p_H = 0.7$ GPa. (**a**) Oil and steel ball heating, (**b**) glass disc heating, (**c**) entire system heating.

In the above analysis, the nominal inlet ambient viscosity is used to describe its contribution to film formation. In fact, the actual inlet ambient is different from the nominal one due to the heat transfer to the oil. To observe the temperature distributions at the inlet region and in the contacts, Figure 8 illustrates the temperature profiles in the middle layer of the film on the $Y = 0$ section. Three distinct entrainment speeds are chosen to represent low, moderate, and high velocities. Again, three

heating methods and three SRRs are employed. Prior to oil entrainment into the contact region, variations in temperature along the X direction differ depending on the heating method employed. In Figure 8a, a decreasing trend followed by an increasing trend is observed due to higher oil temperatures compared to those of the disc surface. Heat transfer occurs from the oil to the disc body until reaching a final equilibrium state. With increasing speed, there is a shift in position towards the contact region for the location of minimal temperature. The opposite temperature variations observed in Figure 8b can be attributed to the reverse heat transfer occurring from the disc to the oil. In Figure 8c, a constant oil temperature is maintained due to the absence of any heat exchange between the oil and solid surfaces. Since the inlet ambient viscosity determines the film formation and the pressure begins to establish in the inlet convergent gap, the actual oil temperatures are listed in Table 4 to show the influence of heat transfer. It can be seen that in the case of $t_0 = t_b = 75$ °C and $t_d = 25$ °C, the oil temperature ranges from 55.39 °C to 69.60 °C for all speeds, which is lower than the nominal temperature of 75 °C due to the heat transfer to the disc surface. From Figure 3, it is evident that viscosity decreases within the range of 55.39 °C to 75 °C, with corresponding values ranging from 37.5 mPa·s to 15 mPa·s. When $t_0 = t_b = 25$ °C and $t_d = 75$ °C, the oil temperature ranges from 33.05 °C to 45.69 °C, with the corresponding viscosity ranging from 125 mPa·s to 75 mPa·s, which is much higher compared to the case of $t_0 = t_b = 75$ °C and $t_d = 25$ °C, but a similar film thickness magnitude as the case of $t_0 = t_b = 75$ °C and $t_d = 25$ °C is maintained. This confirms that the temperature gradient effect plays crucial a role in establishing the film thickness in the case of oil and ball heating. No obvious temperature change is found in the case of entire system heating, where the low ambient viscosity results in a low film thickness.

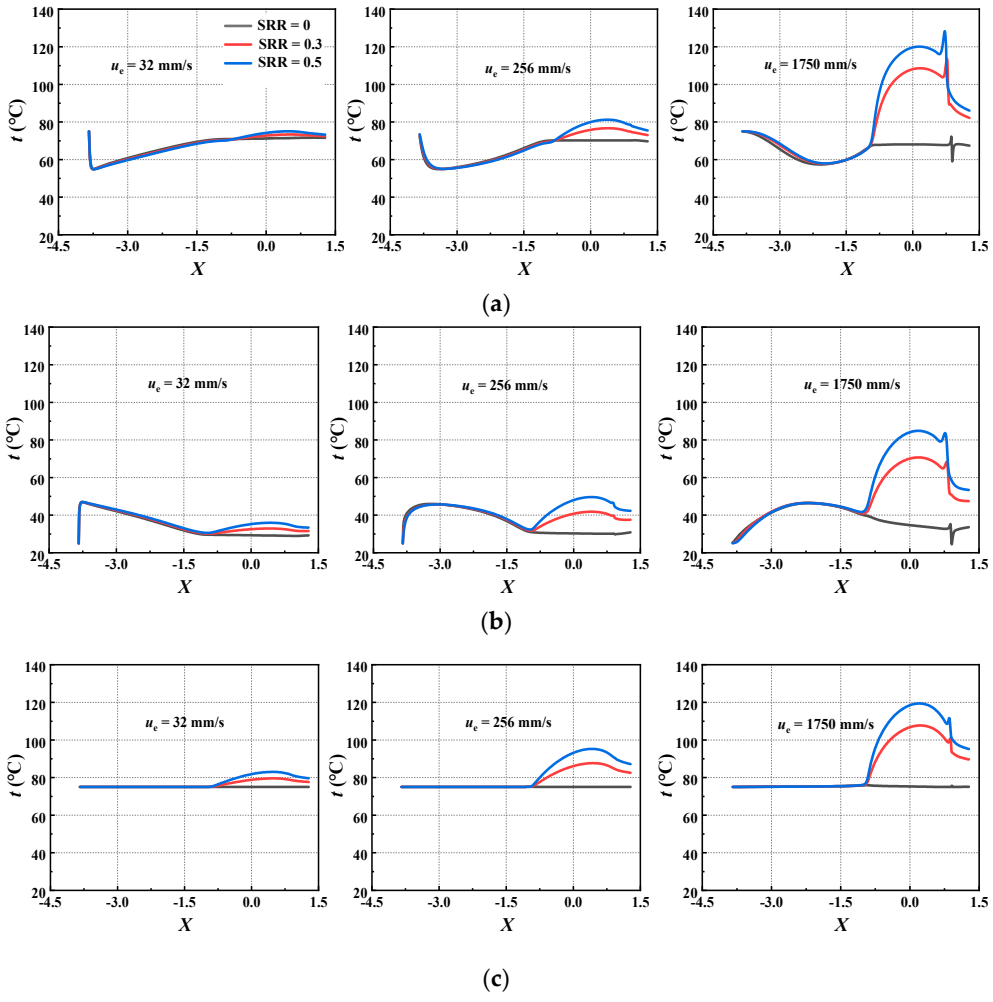

Figure 8. Profiles of temperature in the middle layer of the film on $Y = 0$ section at three speeds under different SRRs, $p_H = 0.7$ GPa. (**a**) Oil and steel ball heating, $t_0 = t_b = 75$ °C, $t_d = 25$ °C; (**b**) glass disc heating, $t_0 = t_b = 25$ °C, $t_d = 75$ °C; (**c**) entire system heating, $t_0 = t_b = t_d = 75$ °C.

Table 4. Oil temperatures at inlet region, SRR = 0.5.

Nominal Temperature Conditions (°C) @ Speed	Actual Oil Temperature (°C) @ $X = -3.0$	Actual Oil Temperature (°C) @ $X = -1.5$	Actual Oil Temperature (°C) @ $X = -1.0$
$t_0 = t_b = 75$, $t_d = 25$ @ $u_e = 32$ mm/s	57.29	67.10	69.60
$t_0 = t_b = 75$, $t_d = 25$ @ $u_e = 256$ mm/s	55.39	62.77	68.99
$t_0 = t_b = 75$, $t_d = 25$ @ $u_e = 1750$ mm/s	68.49	59.79	66.43
$t_0 = t_b = 25$, $t_d = 75$ @ $u_e = 32$ mm/s	42.94	33.05	30.58
$t_0 = t_b = 25$, $t_d = 75$ @ $u_e = 256$ mm/s	45.69	37.93	32.37
$t_0 = t_b = 25$, $t_d = 75$ @ $u_e = 1750$ mm/s	41.42	44.51	41.95
$t_0 = t_b = t_d = 75$ @ $u_e = 32$ mm/s	75.00	75.00	75.00
$t_0 = t_b = t_d = 75$ @ $u_e = 256$ mm/s	75.00	75.02	75.09
$t_0 = t_b = t_d = 75$ @ $u_e = 1750$ mm/s	75.11	75.45	76.27

After the oil enters the contacts, it becomes evident that the overall temperature of the oil film increases with both entrainment speed and SRR. At SRR = 0, where no shear is imposed on the film, the temperature remains relatively constant except in cases involving glass disc heating (u_e = 1750 mm/s). In Figure 7b, at u_e = 1750 mm/s, the decrease in temperature can be attributed to the high thermal conductivity of steel and the limited time for heat transfer from the glass surface to the oil. With a given speed, an increase in SRR leads to an enlargement of Δu (the speed difference between bounding surfaces), resulting in a rise in temperature. For instance, at SRR = 0.5, an increase in entrainment speed also amplifies Δu, as shown in Table 5, which contributes to an elevation in temperature.

Table 5. Speeds and speed differences under different SRRs.

SRR	u_e (mm/s)	u_d (mm/s)	u_b (mm/s)	Δu (mm/s)
0	32	32	32	0
0	256	256	256	0
0	1750	1750	1750	0
0	2500	2500	2500	0
0.3	32	36.8	27.2	9.6
0.3	256	294.4	217.6	76.8
0.3	1750	2012.5	1487.5	525
0.3	2500	2875	2125	750
0.5	32	40	24	16
0.5	256	320	192	128
0.5	1750	2187.5	1312.5	875
0.5	2500	3125	1875	1250

In the above observations and discussions, the thermal-viscosity wedge effect induced by in-contact shear is not prominently observed, due to the relatively small value of the SRR, which is also evident from Figure 4 where only a slight dimple appears. To investigate the influence of the thermal-viscosity wedge effect on film formation, Figure 9 presents the film thickness at SRR = 1.0 under three heating methods, with the corresponding results at SRR = 0.5 indicated by dashed lines. It is observed that when employing an entire system heating approach that mainly relies on a pure thermal-viscosity wedge effect, the resulting film thickness exceeds that obtained at SRR = 0.5. This suggests that higher values of SRR enhance the thermal-viscosity wedge effect. However, when using disc heating, there is almost no change in film thickness as the SRR increases from 0.5 to 1.0, indicating that a greater amount of thin lubricant is entrained into the contacts by

the disc to counterbalance any positive effects arising from thermal viscosity wedging. In contrast, a larger value of SRR leads to a significant increase in film thickness as a greater amount of thick lubricant is drawn into contact with the low-temperature discs.

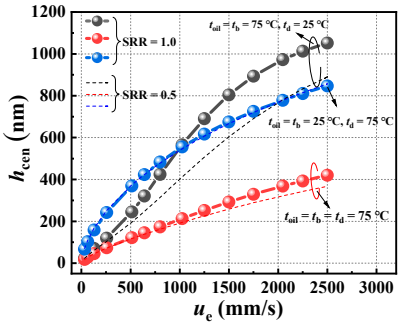

Figure 9. Variations in film thickness with speed at different oil and solid temperatures, p_H = 0.7 GPa, SRR = 1.0.

Figure 10 illustrates the profiles of oil temperature and the corresponding film at SRR = 1.0. Similar trends are observed as in Figure 8, where the temperature increases in the contacts with speed due to the increase in Δu. At low speed (u_e = 32 mm/s), film thickness corresponds to inlet oil temperature; lower inlet temperatures result in higher film thicknesses. As the speed increases to u_e = 1024 mm/s, the entire system heating method yields the lowest film thickness due to the highest inlet temperature. Although the disc heating method has the lowest inlet temperature, its film thickness is similar to that of the oil and ball heating method. Furthermore, for the entire system heating case, the film profile cannot maintain a parallel shape, as seen at u_e = 32 mm/s, but presents a concave shape instead. In the case of oil and ball heating, an obvious central dimple shape forms due to the external thermal gradient effect. At elevated speeds (u_e = 2500 mm/s), the central dimple shape becomes more pronounced for the entire system heating case, indicating an enhancement in the thermal-wedge effect. Despite possessing higher inlet temperatures than the disc heating method, oil and ball heating produces the highest film thickness with a remarkable dimple, indicating a significant temperature gradient effect.

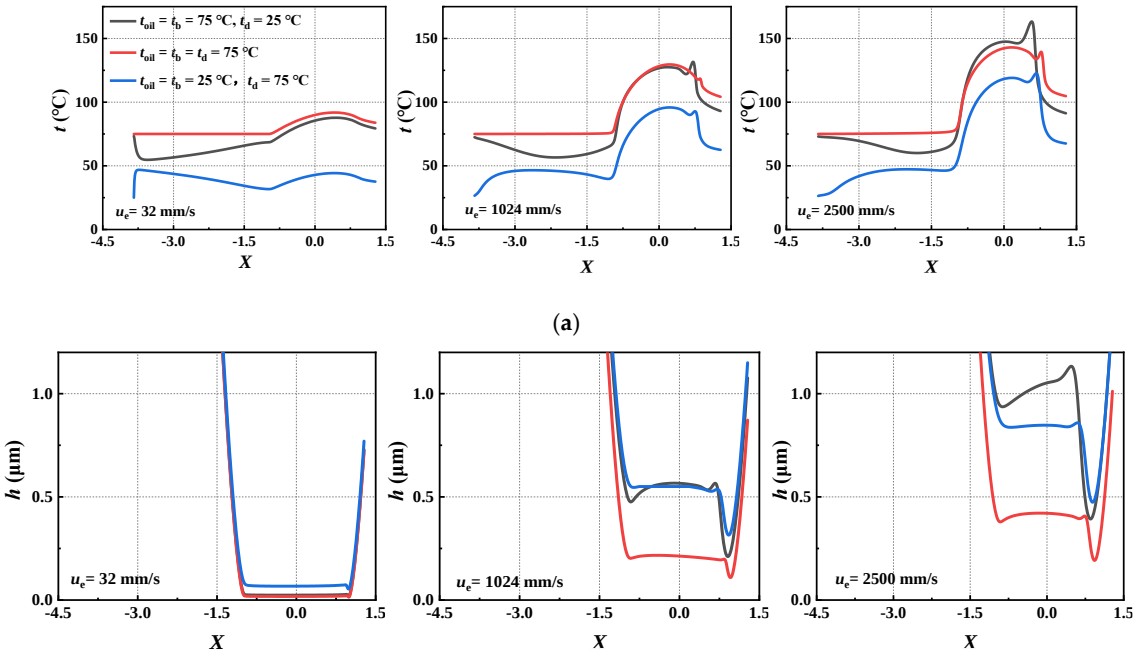

(**a**)

(**b**)

Figure 10. Profiles of oil temperature and lubricating film on $Y = 0$ section under the three heating methods, p_H = 0.7 GPa, SRR = 1.0. (**a**) Profiles of the temperature in the middle layer of the film, (**b**) profiles of the EHL film.

In practical applications, steel is the predominant material used for mechanical components such as rolling bearings. If the contact body made of glass material is replaced with steel and uses the corresponding steel parameters (C_d = 470 J/kg·K, ρ_d = 7850 kg/m^3, and E' = 226 GPa), Figure 11 illustrates the variations in film thickness with speed under the same conditions shown in Figure 9. It is evident that when oil and ball heating occur, there is a significant increase in film thickness to high values, indicating a more pronounced temperature gradient effect. Similarly, an obvious increase in film thickness is observed in the disc heating case, suggesting that the temperature gradient effect also plays an important role in steel–steel contacts. However, when the entire system heats up, the film thickness decreases due to more efficient heat dissipation and the absence of thermal-viscosity edge formation. In practical engineering cases, temperature differences between contact surfaces may commonly arise from various factors such as asymmetrical system cooling or other sources. The findings demonstrate that the presence of a temperature difference, particularly when the cooler surface moves faster, exerts an obvious influence on both film formation and subsequent lubrication state, as well as rheological behaviors of EHL films.

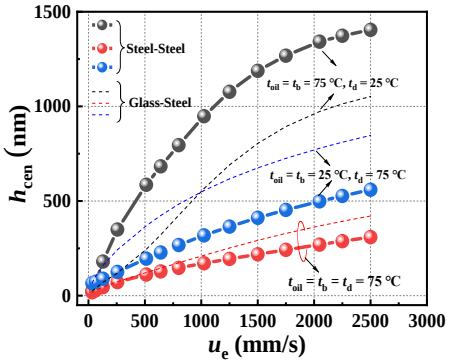

Figure 11. Variations of film thickness with speed at different oil and solid temperatures, steel–steel contact, p_H = 0.7 GPa, SRR = 1.0.

5. Conclusions

The motivation for this study originates from the ball-on-disc experimental observations, where an oil and ball heating method was employed. It was discovered that the film thickness deviates from the traditional linear distribution predicted by the Hamrock–Dowson equation. Further analysis reveals that the temperature difference between the contact surfaces significantly influences these results. This observation inspired us to design three different heating methods to investigate how temperature differences affect film formation, with a subsequent comparison of test results against numerical simulations. To gain deeper insights into the underlying mechanisms induced by the temperature difference, extended numerical simulations were conducted under various oil and solid body temperature conditions, while also considering the influence of SRR on the results. The main conclusions are as follows:

(1) To investigate the impact of oil and body temperatures on film formation, three heating methods were employed in both experiments and numerical simulations: oil and ball heating, disc heating, and entire system heating. Overall, the measured film thicknesses were higher than those obtained from numerical results due to heat transfer to the surroundings. Both cases demonstrate the influence of heating methods on film formation as well as the validity of the numerical model.

(2) The numerical results demonstrate that in the case of oil and ball heating, the temperature gradient induced by the temperature difference between the disc and ball plays a crucial role in film formation, significantly surpassing the conventional thermal-viscosity wedge effect. This effect is further enhanced at high SRR or in steel–steel contacts. However, when it comes to disc heating, the temperature gradient is not prominent, due to the ineffective entrainment of thick oil to the contacts by the ball surface, resulting in a nearly constant film thickness at different SRRs.

(3) The overall film formation is primarily governed by the oil inlet temperature, which determines the ambient viscosity at the inlet. Meanwhile, the local film formation, characterized by a dimple shape, is influenced by both the thermal gradient effect and thermal-viscosity wedge effect.

(4) The results suggest that the selection of the heating method in experiments should be conducted with caution, or alternatively, strict control over temperature conditions is necessary to ensure the integrity of test results. Temperature variations commonly occur in practical components,

which can impact both film formation and the rheological properties of lubricating films. Future research will investigate the effects of oil and solid body temperatures on EHL film rheology.

Author Contributions: Conceptualization, X.L.; investigation, J.G., Y.T., Z.C. and X.Y.; methodology, P.Y. and X.J.; validation, X.L.; writing—original draft, J.G.; writing—review and editing, X.L. All authors have read and agreed to the published version of the manuscript.

Funding: This research is funded by the National Natural Science Foundation of China (No. 52275196) and the Youth Innovation and Technology Support Program of Shandong Province (No. 2019KJB010).

Data Availability Statement: The data used to support the findings of this study are included in the manuscript.

Conflicts of Interest: Author Xinming Li was employed by the company Shandong Zhilian Community Bearing Technology Co., Ltd. The remaining authors declare that the research was conducted in the absence of any commercial or financial relationships that could be construed as a potential conflict of interest.

References

1. Takabi, J.; Khonsari, M. On the thermally-induced seizure in bearings: A review. *Tribol. Int.* **2015**, *91*, 118–130. [CrossRef]
2. Cui, L.; Zhang, H.S. Limiting speeds of high-speed ball bearings considering prevention of skidding and overheating conditions. *Adv. Mech. Eng.* **2019**, *11*, 1–11. [CrossRef]
3. Morales-Espejel, G.E.; Gabelli, A. A model for rolling bearing life with surface and subsurface survival: Surface thermal effects. *Wear* **2020**, *460–461*, 203446. [CrossRef]
4. Zhou, X.W.; Zhang, H.; Hao, X.; Liao, X.; Han, Q.K. Investigation on thermal behavior and temperature distribution of bearing inner and outer rings. *Tribol. Int.* **2018**, *130*, 289–298. [CrossRef]
5. Jiang, S.; Mao, H. Investigation of the high speed rolling bearing temperature rise with oil-air lubrication. *J. Tribol.* **2011**, *133*, 021101. [CrossRef]
6. Lugt, P.M. Modern advancements in lubricating grease technology. *Tribol. Int.* **2016**, *97*, 467–477. [CrossRef]
7. Peretiaka, N.; Boryak, K.; Vatrenko, O. Improving the thermal method for assessing the technical condition of rolling bearings based on the heating rate criterion. *East. Eur. J. Enterp. Technol.* **2020**, *5*, 118–126. [CrossRef]
8. Omasta, M.; Adam, J.; Sperka, P.; Krupka, I.; Hartl, M. On the temperature and lubricant film thickness distribution in EHL contacts with arbitrary entrainment. *Lubricants* **2018**, *6*, 101. [CrossRef]
9. Habchi, W.; Eyheramendy, D.; Bair, S.; Vergne, P. Thermal elastohydrodynamic lubrication of point contacts using a newtonian/generalized newtonian lubricant. *Tribol. Lett.* **2008**, *30*, 41–52. [CrossRef]
10. Lu, J.; Reddyhoff; Dini, D. A study of thermal effects in EHL rheology and friction using infrared microscopy. *Tribol. Int.* **2020**, *146*, 106179. [CrossRef]
11. Liu, H.; Zhang, B.; Bader, N.; Poll, G.; Venner, C. Influences of solid and lubricant thermal conductivity on traction in an EHL circular contact. *Tribol. Int.* **2020**, *146*, 106059. [CrossRef]
12. Wang, H.; Qian, S.; Ni, Z.; Huang, C.; Zhao, Y. Experimental investigation on the rheological properties of castor oil at different temperatures. *Proc. Inst. Mech. Eng. Part J J. Eng. Tribol.* **2018**, *232*, 861–870. [CrossRef]
13. White, B.; Lewis, R. Simulation and understanding the wet-rail phenomenon using twin disc testing. *Tribol. Int.* **2019**, *136*, 475–486. [CrossRef]
14. Liu, H.C.; Zhang, B.B.; Bader, N.; Venner, C.H.; Poll, G. Simplified traction prediction for highly loaded rolling/sliding EHL contacts. *Tribol. Int.* **2020**, *148*, 106335. [CrossRef]
15. Hamrock, B.J.; Dowson, D. Isothermal elastohydrodynamic lubrication of point contacts: Part II—Ellipticity parameter results. *J. Lubr. Technol.* **1976**, *98*, 375–381. [CrossRef]
16. Bair, S. Shear thinning correction for rolling/sliding elastohydrodynamic film thickness. *Proc. Inst. Mech. Eng. Part J J. Eng. Tribol.* **2005**, *219*, 69–74. [CrossRef]
17. Hartinger, M.; Dumont, M.; Ioannides, S.; Gosman, D.; Spikes, H. CFD modeling of a thermal and shear-thinning elastohydrodynamic line contact. *J. Tribol.* **2008**, *130*, 041503. [CrossRef]
18. Yagi, K.; Kyogoku, K.; Nakahara, T. Relationship between temperature distribution in EHL film and dimple formation. *J. Tribol.* **2005**, *127*, 658–665. [CrossRef]
19. Yagi, K.; Sugimura, J.; Vergne, P. Rheological response of fatty alcohols in sliding elastohydrodynamic contacts. *Tribol. Int.* **2012**, *49*, 58–66. [CrossRef]
20. Zhang, B.B.; Wang, J.; Omasta, M.; Kaneta, M. Variation of surface dimple in point contact thermal EHL under ZEV condition. *Tribol. Int.* **2016**, *94*, 383–394. [CrossRef]
21. Björling, M.; Habchi, W.; Bair, S.; Larsson, R.; Marklund, P. Towards the true prediction of EHL friction. *Tribol. Int.* **2013**, *66*, 19–26. [CrossRef]

22. Zhu, D.; Wen, S.Z. A full numerical solution for the thermoelastohydrodynamic problem in elliptical contacts. *J. Tribol.* **1984**, *106*, 246–254. [CrossRef]
23. Kim, H.J.; Ehret, P.; Dowson, D.; Taylor, C.M. Thermal elastohydrodynamic analysis of circular contacts part 2: Non-Newtonian model. *Proc. Inst. Mech. Eng. Part J J. Eng. Tribol.* **2001**, *215*, 353–362. [CrossRef]
24. Kim, K.H.; Sadeghi, F. Three-dimensional temperature distribution in EHD lubrication: Part II—Point contact and numerical formulation. *J. Tribol.* **1993**, *115*, 36–45. [CrossRef]
25. Habchi, W.; Vergne, P.; Bair, S.; Andersson, O.; Eyheramendy, D.; Morales-Espejel, G.E. Influence of pressure and temperature dependence of thermal properties of a lubricant on the behaviour of circular TEHD contacts. *Tribol. Int.* **2010**, *43*, 1842–1850. [CrossRef]
26. Doki-Thonon, T.; Fillot, N.; Morales Espejel, G.E.; Querry, M.; Philippon, D.; Devaux, N.; Vergne, P. A dual experimental/numerical approach for film thickness analysis in TEHL spinning skewing circular contacts. *Tribol. Lett.* **2013**, *50*, 115–126. [CrossRef]
27. Guo, F.; Yang, P.; Qu, S. On the theory of thermal elastohydrodynamic lubrication at high slide-roll ratios-circular glass-steel contact solution at opposite sliding. *J. Tribol.* **2001**, *123*, 816–821. [CrossRef]
28. Nakahara, T.; Yagi, K. Influence of temperature distributions in EHL film on its thickness under high slip ratio conditions. *Tribol. Int.* **2007**, *40*, 632–637. [CrossRef]
29. Reddyhoff, T.; Spikes, H.A.; Olver, A.V. Improved infrared temperature mapping of elastohydrodynamic contacts. *Proc. Inst. Mech. Eng. Part J J. Eng. Tribol.* **2009**, *223*, 1165–1177. [CrossRef]
30. Le Rouzic, J.; Reddyhoff, T. Development of infrared microscopy for measuring asperity contact temperatures. *J. Tribol.* **2013**, *135*, 021504. [CrossRef]
31. Lu, J.; Reddyhoff, T.; Dini, D. 3D measurements of lubricant and surface temperatures within an elastohydrodynamic contact. *Tribol. Lett.* **2018**, *66*, 7. [CrossRef] [PubMed]
32. Liu, H.C.; Zhang, B.B.; Bader, N. Crucial role of solid body temperature on elastohydrodynamic film thickness and traction. *Tribol. Int.* **2019**, *131*, 386–397. [CrossRef]
33. Campos, A.; Sottomayor, A.; Seabra, J. Non-newtonian thermal analysis of an EHD contact lubricated with MIL-L-23699 oil. *Tribol. Int.* **2006**, *39*, 1732–1744. [CrossRef]
34. Liu, X.; Yang, P. Influence of solid body temperature on the thermal EHL behavior in circular contacts. *J. Tribol.* **2008**, *130*, 014501. [CrossRef]
35. Yang, P.; Liu, X. Effects of solid body temperature on the Non-Newtonian thermal elastohydrodynamic lubrication behaviour in point contacts. *Proc. Inst. Mech. Eng. Part J J. Eng. Tribol.* **2009**, *223*, 959–969. [CrossRef]
36. Liu, H.C.; Guo, F.; Guo, L.; Wong, P.L. A dichromatic interference intensity modulation approach to measurement of lubricating film thickness. *Tribol. Lett.* **2015**, *58*, 15. [CrossRef]
37. Cui, J.L.; Yang, P. A further investigation on the viscosity-density relation of lubricant and a quantitative numerical analysis for the generalized newtonian thermal EHL problem. *Tribology* **2016**, *36*, 679–686.
38. Hamrock, B.J.; Dowson, D. Isothermal elastohydrodynamic lubrication of point contacts: Part III—Fully flooded results. *J. Lubr. Technol.* **1977**, *99*, 264–275. [CrossRef]